

Description of ϕ -meson production in hadronic and nuclear collisions at very high energies

G.H. Arakelyan¹, C. Merino², Yu.M. Shabelski³

¹A.Alikhanyan National Scientific Laboratory
(Yerevan Physics Institute)
Yerevan, 0036, Armenia
e-mail: argev@mail.yerphi.am

²Departamento de Física de Partículas, Facultade de Física
and Instituto Galego de Física de Altas Enerxías (IGFAE)
Universidade de Santiago de Compostela
15782 Santiago de Compostela
Galiza-Spain
e-mail: merino@fpaxp1.usc.es

³Petersburg Nuclear Physics Institute
NCR Kurchatov Institute
Gatchina, St.Petersburg 188350, Russia
e-mail: shabelsk@thd.pnpi.spb.ru

Abstract

We expose the current experimental and theoretical situation of the interesting case of the production of ϕ mesons in up to very high energy collisions of hadrons on both nucleon and nuclear targets, and we present a quantitatively good theoretical description of the corresponding experimental data, based on the formalism of the well established Quark-Gluon String Model, that has proved to be valid for a wide energy range. All the available experimental data for ϕ -meson production in hadron-nucleon collisions on the spectra of secondary ϕ , and on the ratios of ϕ/π^- and ϕ/K^- production cross sections, as well the corresponding ones for ϕ -meson production on nuclear targets, are considered. In particular, it is seen that the production of ϕ -mesons on nuclear targets presents unusually small shadow corrections for the inclusive density in the central rapidity region.

1 Introduction

The ϕ -meson is a system of $s\bar{s}$ quarks, and though s and \bar{s} quarks have non-zero masses, at the same time their masses are not large enough to make standard perturbative Quantum Chromodynamics (QCD) applicable. Thus, one could think of treating the ϕ -meson as an intermediate case between soft and hard physics, making it especially

interesting to disentangle the open question of the overlap and transition between the soft (non-perturbative) and the hard (perturbative) regimes. At the same time, the ϕ -meson is rarely produced, and it can be sensitive to the production mechanism.

Here we update and complete the theoretical description, already presented in references [1, 2], of the experimental data on production of vector ϕ -mesons a rarely produced system formed of s quark and \bar{s} antiquark, with non-zero masses, in hadron-nucleon, hadron-nucleus, and nucleus-nucleus collisions for a large energy region, by including newly published experimental data in the analysis.

For that, we use the Quark-Gluon String Model (QGSM) [3, 4] formalism, that allows one to make quantitative predictions on the inclusive densities of different secondaries. In particular, the description of the experimental data on the production of pseudoscalar mesons π and K and baryons p , \bar{p} , Λ , and $\bar{\Lambda}$ was obtained in [5, 6, 7, 8, 9], and the same for the production of vector mesons [10, 11], and of hyperons, including the multistrange ones [12, 13], both in the central and beam fragmentation regions. Thus, the QGSM provides a consistent description of multiparticle production processes in hadron-nucleon [3, 4], hadron-nucleus [14, 15], and nucleus-nucleus [16, 17] collisions up to the currently available high energies of the Relativistic Heavy Ion Collider-RHIC (BNL-USA) and the Large Hadron Collider-LHC (CERN-Switzerland).

The QGSM analysis gives a quantitatively consistent description of the spectra of secondary ϕ mesons, as well as of the ratios of ϕ/π^- and ϕ/K^- production cross sections in pp -collisions for a large scope of the initial energy going up to the RHIC and LHC ranges. In the case of collisions with a nuclear target, the description of the experimental data is also quantitatively good for both the initial energy dependence and the A -dependence of the produced ϕ -mesons, and, in particular, a natural explanation appears for the unusually small shadow corrections experimentally observed in proton-nucleus and nucleus-nucleus collisions at very high energies for the inclusive density [7, 12, 18, 19] (saturation of the inclusive density) in the central rapidity region.

2 Inclusive meson production in the QGSM formalism

In order to obtain quantitative results in describing inclusive secondary-hadron spectra integrated over the secondary-particle transverse momentum, p_T , a model for multiparticle production is needed. It is for that purpose that we have used the QGSM [3, 4] in the numerical calculations presented here.

The QGSM [3, 4, 14] is a model based on the Dual Topological Unitarization (DTU), Regge phenomenology, and nonperturbative notions of QCD that successfully predicts and describes many features of the hadronic processes in a wide energy range. In particular, the QGSM allows one to make quantitative predictions on the inclusive

densities of different secondaries, both in the central and the beam fragmentation regions.

In the QGSM frame, high energy hadron-nucleon collisions are considered as taking place via the exchange of one or several Pomerons. Each Pomeron is considered in DTU as a cylinder-type diagram (Fig. 1a), in which the cylinder boundaries are drawn by the dash-dotted vertical lines. The surface of the cylinder is schematically depicted by dashed lines, while the solid lines at the top and bottom of the cylinder represent, respectively, the beam and the target quarks, which interaction is mediated by the Pomeron exchange.

The cut [20] between Pomerons in a multipomeron diagram results in elastic or diffraction dissociation processes, while the cut through one (Fig. 1b) or several (Fig. 1c) Pomerons corresponds to inelastic processes with multiple production of secondaries, the cut of every Pomeron leading to the production of two showers of secondaries.

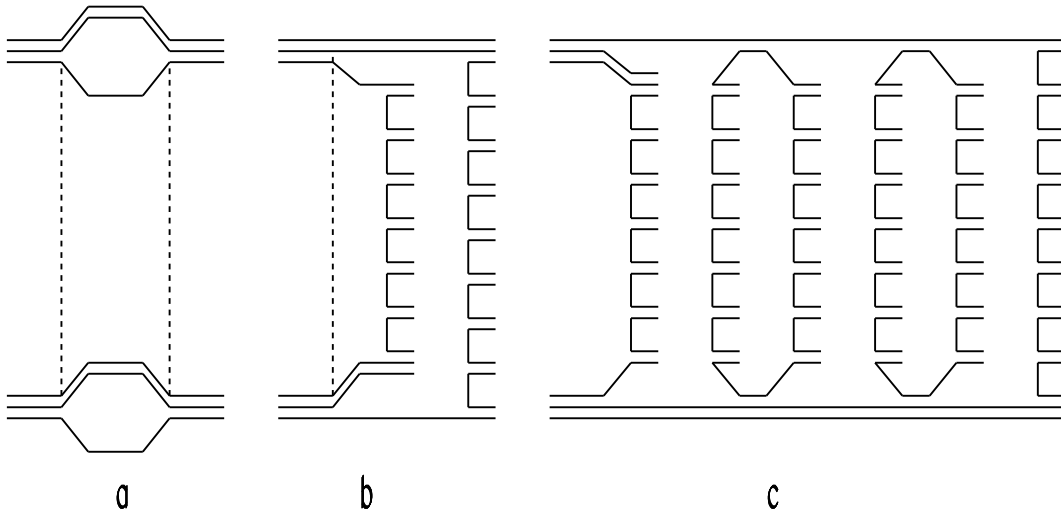


Figure 1: (a) Cylinder-type diagram representing a Pomeron exchange within the DTU classification (the solid lines represent quarks), (b) cut of the cylinder-type diagram corresponding to the contribution of one-Pomeron exchange to inelastic pp scattering, and (c) the cuts of one of the diagrams for the inelastic interaction of the incident proton with the target proton in a pp collision.

For a nucleon target, the inclusive rapidity, y , or Feynman- x , x_F , spectra of a secondary hadron h have the form [3]:

$$\frac{dn_h}{dy} = \frac{x_E}{\sigma_{inel}} \cdot \frac{d\sigma}{dx_F} = \sum_{n=1}^{\infty} w_n \cdot \phi_n^h(x) , \quad (1)$$

where $x_E = E/E_{max}$, the functions $\phi_n^h(x)$ determine the contribution of diagrams with n cut Pomerons and w_n is the relative weight of these diagrams, which is calculated as

$$w_n = \sigma^n / \sigma_{inel} , \quad (2)$$

with $\sigma_{inel} = \sigma_{tot} - \sigma_{el}$.

The cross sections of all inelastic processes corresponding to diagrams where $n \geq 1$ Pomerons are cutted can be calculated [21] with the help of the AGK cutting rules [20]:

$$\sigma_{hN}^{(n)} = \frac{\sigma_P}{n \cdot z} \left(1 - e^{-z} \sum_{k=1}^{n-1} \frac{z^k}{k!} \right). \quad (3)$$

The average number of exchanged Pomerons in pp collisions $\langle n \rangle_{pp}$ slowly increases with the energy.

The parametrization of the Pomeron pole and the calculation of the corresponding elastic and inelastic cross sections, are presented in Appendix A, together with a detailed list of the corresponding references.

The inclusive spectrum of secondaries is then determined by the convolution of diquark, valence quark, and sea quark distributions in the incident particles, $u(x, n)$, with the fragmentation functions of quarks and diquarks into the secondary hadrons, $G(z)$. The distribution functions, $u(x, n)$, and the fragmentation functions, $G(z)$, are determined by the appropriate Reggeon diagrams [4, 14, 22], and both are constructed using the Reggeon counting rules [22].

The diquark and quark distribution functions depend on the number n of cut Pomerons in the diagrams being considered. The parametrization of distribution functions of quarks and diquarks in colliding particles were obtained in [1, 14], and they are presented in the Appendix B.

The parametrizations of quark and diquark fragmentation functions to ϕ -mesons, together with the normalization parameter a_ϕ , were given in [1, 10] and they are presented here in Appendix C. The value of the parameter $a_\phi = 0.11$ was determined from comparison with low energy experimental data, and it has been used in the theoretical calculations for the whole energy region under consideration.

Note that the quark-antiquark distribution functions $u(x, n)$ differ from the standard *PDF* distributions extracted from a fit to experimental data, since the functions $u(x, n)$ are applicable at the rather low Q^2 which correspond to soft processes, whereas the *PDF* distributions resulted from describing high- Q^2 processes.

For pp collisions, one has

$$\begin{aligned} \phi_n^h(x) &= f_{qq}^h(x_+, n) \cdot f_q^h(x_-, n) + f_q^h(x_+, n) \cdot f_{qq}^h(x_-, n) \\ &+ 2(n-1) \cdot f_s^h(x_+, n) \cdot f_s^h(x_-, n) \quad , \end{aligned} \quad (4)$$

$$x_\pm = \frac{1}{2} [\sqrt{4m_T^2/s + x^2} \pm x] \quad , \quad (5)$$

where $m_T = \sqrt{m^2 + p_T^2}$ is the transverse mass of the product hadron and f_{qq} , f_q , and f_s represent the contributions of, respectively, diquarks, valence quarks and antiquarks,

and sea quarks and antiquarks [4, 22]. In the case of meson-nucleon collisions, the diquark contribution $f_{qq}^h(x_+, n)$ in Eq. (4) should be replaced by the valence antiquark contribution $f_{\bar{q}}^h(x_+, n)$.

The functions f_{qq} , f_q , $f_{\bar{q}}$, and f_{sea} are determined by the convolution of the diquark, quark, and antiquark distribution functions, $u(x, n)$, with the fragmentation functions to hadron h , $G^h(z)$, e.g.,

$$f_i^h(x_+, n) = \int_{x_+}^1 u_i(x_1, n) G_i^h(x_+/x_1) dx_1, \quad (6)$$

where i stands for diquarks (qq), valence and sea quarks (q), and valence and sea antiquarks (\bar{q}). The details of the model are presented in [3, 4, 5, 6, 12].

To describe the nucleon interaction with nuclear targets, use is made of Gribov-Glauber multiple-scattering theory. It permits considering collisions with nuclei as a superposition of interactions involving various numbers of target nucleons [23, 24, 25, 26].

In the case of nucleus-nucleus collisions, this approach makes it possible to consider this interaction as a superposition of individual nucleon-nucleon interactions. Although an analytic summation of all diagrams is impossible in this case [27], the most important classes of diagrams can be summed analytically in the so-called rigid nucleus approximation [28], that we use here.

In calculating inclusive spectra of secondary particles produced in pA collisions, we should consider the possibility of cutting one or several Pomerons in each of the ν blocks of the inelastic proton-nucleon interaction.

For example, Fig. 2 shows one of the diagrams that contribute to the inelastic interaction of a beam proton with two target nucleons. One Pomeron is cut in the proton-nucleon₁ interaction block, and two Pomerons are cut in the proton-nucleon₂ interaction block.

The process shown in Fig. 2 satisfies the condition that the absorptive part of the hadron-nucleus amplitude is determined by the combination of the absorptive parts of the hadron-nucleon amplitude [23, 24, 25, 26].

The contribution of the diagram in Fig. 2 to the inclusive cross sections has the form

$$\begin{aligned} \frac{x_E}{\sigma_{prod}^{pA}} \cdot \frac{d\sigma}{dx_F} &= 2 \cdot W_{pA}(2) \cdot w_1^{pN_1} \cdot w_2^{pN_2} \cdot \left\{ f_{qq}^h(x_+, 3) \cdot f_q^h(x_-, 1) + \right. \\ &+ f_q^h(x_+, 3) \cdot f_{qq}^h(x_-, 1) + f_s^h(x_+, 3) \cdot [f_{qq}^h(x_-, 2) + f_q^h(x_-, 2) + \\ &+ 2 \cdot f_s^h(x_-, 2)] \left. \right\}, \quad (7) \end{aligned}$$

where $W_{pA}(2)$ is the probability for the interaction of the proton beam with two target nucleons.

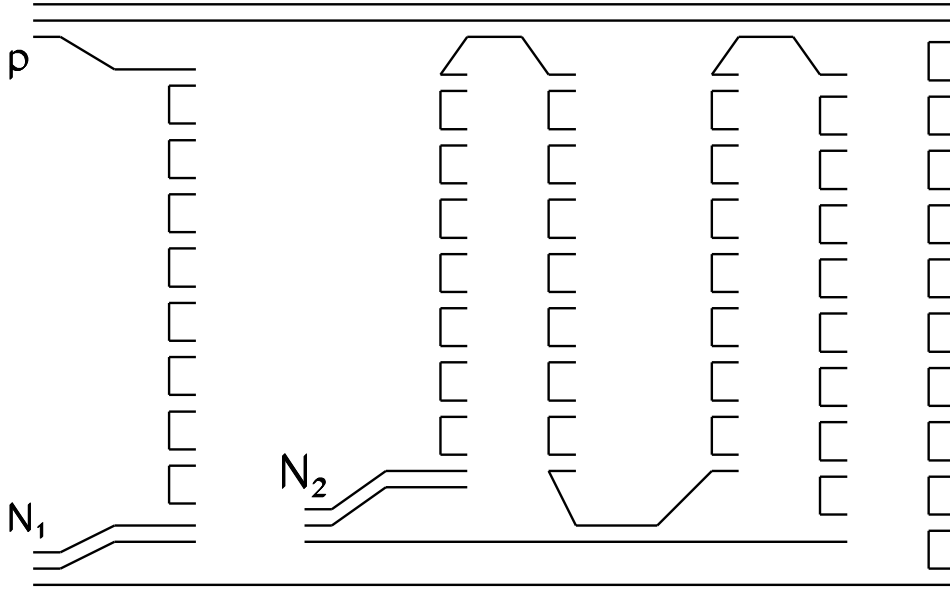


Figure 2: One of the diagrams corresponding to the inelastic interaction of one incident nucleon with two target nucleons N_1 and N_2 in a pA collision.

According to multiple-scattering theory, one has:

$$W_{pA}(\nu) = \sigma^{(\nu)} / \sigma_{prod}^{pA} \quad (8)$$

(see [7] for numerical examples). Here,

$$\sigma^{(\nu)} = \frac{1}{\nu!} \int d^2b \cdot [\sigma_{inel}^{pN} \cdot T(b)]^\nu \cdot e^{-\sigma_{inel}^{pN} \cdot T(b)} \quad , \quad (9)$$

while σ_{prod}^{pA} is the cross section for the production of secondary particles in pA collisions.

It is important to take into account all diagrams featuring all possible configurations of Pomerons and their respective permutations. The quark and diquark distributions and fragmentation functions are identical to those in the case of pN interaction.

The growth of the total number of interacting Pomerons is given by

$$\langle n \rangle_{pA} \sim \langle \nu \rangle_{pA} \cdot \langle n \rangle_{pN} \quad , \quad (10)$$

where $\langle \nu \rangle_{pA}$ is the average number of inelastic collisions within the target nucleus (about four for heavy nuclei at fixed target energies in the range $10^2 - 10^3 GeV$).

In the case of nucleus-nucleus scattering in the projectile-fragmentation region, we use the approach [16, 29, 30] in which a beam of independent nucleons interacts with the target nucleus, this corresponding to the rigid-target approximation of Glauber's theory [28].

In the target fragmentation region, the beam of independent target nucleons interacts with a projectile nucleus. Thus, these two contributions coincide in the midrapidity region.

If the initial energy is not very high, corrections associated with the energy-conservation law play an important role. This approach was successfully used in [30] to describe π^\pm , K^\pm , p , and \bar{p} production in $PbPb$ collisions at 158 GeV/c per nucleon.

In the case of ϕ -meson production in the midrapidity region, we disregard the contributions of diffractive-dissociation processes.

3 Hadroproduction of ϕ -mesons on proton target

In this section we compare the QGSM calculations with the experimental data on ϕ inclusive cross sections in πp and pp collisions at different energies up to the LHC range.

In the upper panel of Fig. 3 we present the experimental data for the differential cross section $d\sigma/dx_F$ of ϕ -mesons produced in $\pi^\pm p$ collisions at initial momenta of π -mesons 93 [31], and 140 GeV/c [32]. The results of the corresponding QGSM calculations at pion beam momenta 93 and 140 GeV/c are shown by dashed and solid curves, respectively. The theoretical curves are in good agreement with experimental data, both for 93 and 140 GeV/c.

In the lower panel of Fig. 3, the data on ϕ -meson production at the higher pion beam initial momenta of 175, 200, and 360 GeV/c are also presented. We see that the experimental data for these three pion beam momenta are in agreement with the results of the theoretical calculations based on the QGSM shown by solid, dashed, and dashed-dotted curves, respectively. Here, the theoretical curves are in general agreement with the data, except for the small x_F region, where we predict a significant increase of $d\sigma/dx_F$ from 200 to 360 GeV/c that is not seen in the experimental data.

The QGSM description of the experimental data on the x_F dependence of $d\sigma/dx_F$ -spectra of ϕ -mesons in pp -collision measured at 93 [31], 120 and 200 GeV/c [33], and 158 GeV/c [34, 35], is presented in Fig. 4. The solid curve corresponds to the proton beam momenta 93 GeV/c, the dashed curve to 158 GeV/c, and the dashed-dotted curve to 200 GeV/c. The agreement of the theoretical calculation with the data is reasonable at small x_F , at large x_F the experimental data falling down faster than the theory, except for the data at 93 GeV/c, when even at small x_F the agreement is not good. One can appreciate some contradiction between the data on the production of ϕ -mesons in pp (Fig. 4) and those in πp (upper panel of Fig. 3) collisions, obtained both by the same experiment [31]. The results of the calculations based on the QGSM at the NA49 Collaboration energy are in agreement with the Monte Carlo predictions obtained by using the LUCIAE model [36].

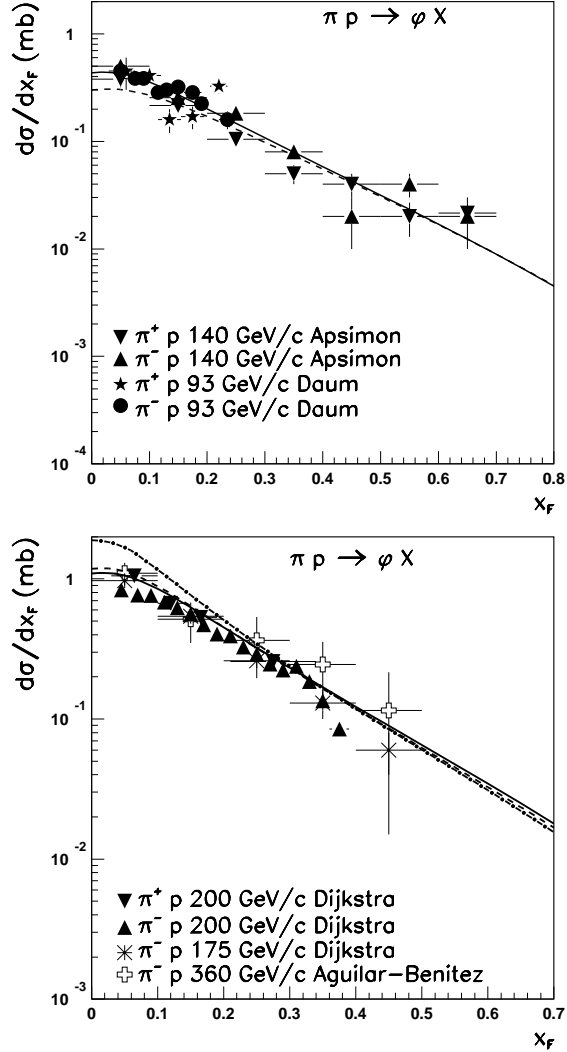


Figure 3: Different experimental data on x_F -spectra of ϕ -mesons produced in $\pi^\pm p$ collisions at different energies [31, 32, 33], compared to the results corresponding calculations based on the QGSM (see the main text for the description of the different experimental data sets and theoretical curves).

In Fig. 5, we compare the QGSM calculations to the experimental data on the inclusive spectra $x_F \cdot d\sigma/dx_F$ of ϕ -mesons in pp -collisions at 400 GeV/c [34, 35]. The agreement of the theoretical curve with the data is good.

In Fig. 6, the rapidity dependence of the density dn/dy of ϕ -mesons produced in pp -collisions at 158 GeV/c [34, 35] is compared to the results of the corresponding calculation based on QGSM (solid curve). The agreement is quite reasonable.

We also compare two new experimental points by ALICE Collaboration on the density dn/dy of ϕ -mesons produced in pp -collisions at 2.76 [37] and 7 TeV [38], with the results of the corresponding QGSM calculations. The dashed curve represents the theoretical results for 2.76 TeV, and the dashed-dotted curve those for 7 TeV. The dotted curve shows the model prediction for 14 TeV.

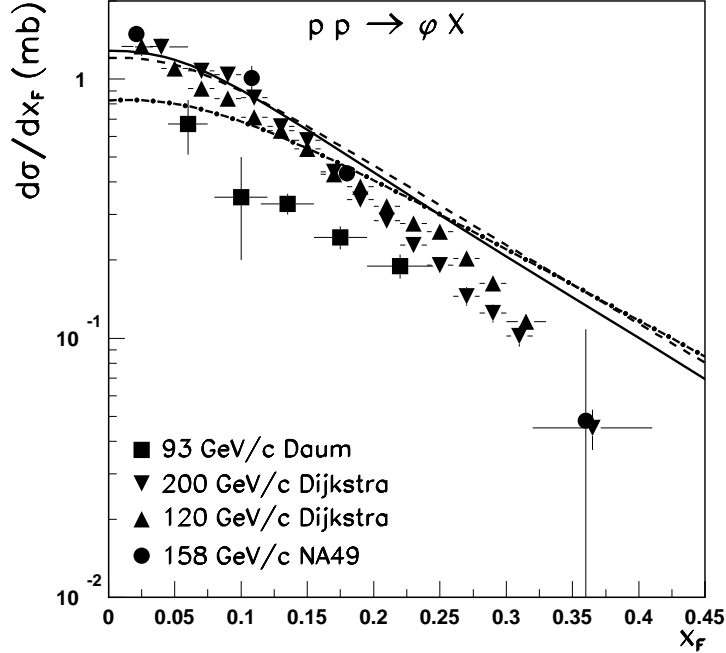


Figure 4: The experimental data [31, 33, 34, 35] on the x_F spectra of ϕ -mesons produced in pp collisions at 93, 120, 158, and 200 GeV/c, compared to the results of corresponding calculations based on the QGSM at 93, 158, and 200 GeV/c.

As it can be seen in Fig. 6, the results of the QGSM calculations are remarkably higher than the experimental data, which were measured for $p_T \geq 0.4$ GeV/c, and extrapolated to $p_T = 0$ [37, 38].

Generally, the QGSM description of the experimental data in the considered energy region shown in Figs. 3–6 is consistent. The description of the large x_F region is rather good in the case of πp collisions, while for pp collisions there is not experimental point at $x_F > 0.35$, except for one point at 400 GeV/c that is in agreement with the QGSM curve.

The QGSM predictions have always been rather reliable for describing π -meson production up to the LHC energies [5, 6, 39]. Thus we have used the published results of the QGSM calculations on π -meson yields to compute the ratios ϕ/π .

The spectra of kaons are presented in Fig. 7. We present the QGSM description of the experimental data on the inclusive spectra of K^+ (upper panel) and K^- (lower panel) mesons in pp -collisions on a wide energy range from $\sqrt{s} = 100$ up to 200 GeV [34, 35, 40]. The integrated over p_T RHIC data at $\sqrt{s} = 200$ GeV have been taken from [34, 35].

We present the results of the QGSM calculations at the two different proton beam momenta (energies): 158 GeV/c ($\sqrt{s} = 17.3$ GeV), by solid curves, and RHIC energy ($\sqrt{s} = 200$ GeV), by dashed curves. For both K^+ and K^- spectra, the QGSM curves are in reasonable agreement with the data. One has to note that some disagreement

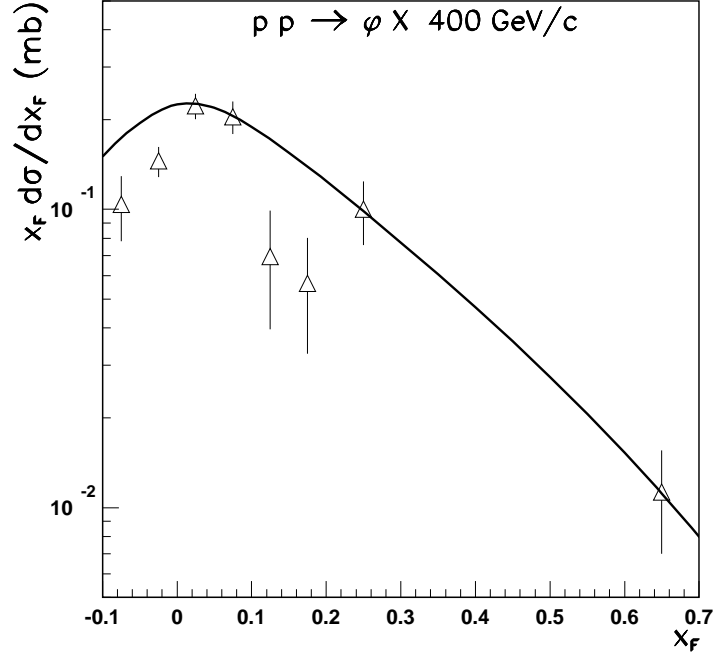


Figure 5: Experimental data [34, 35] on the x_F -spectra of ϕ -mesons produced in pp collisions at a proton beam momentum 400 GeV/c compared to the results of the corresponding QGSM calculation.

between the normalisations of the experimental data by the NA49 Collaboration [34, 35] and of the data at 100 and 175 GeV/c [40] exists. Generally, the experimental spectra of both K^+ and K^- increase with the initial beam momentum (energy), what is in agreement with the results of our calculations.

In the QGSM the calculated density dn/dy is integrated over p_T , so the direct comparison of the results of the calculations based on QGSM to the data would be inconsistent.

In Table 1, the experimental points for the density dn/dy of ϕ -meson inelastic production by the ALICE Collaboration at $\sqrt{s} = 2.76$ [37] and 7 TeV [38], are compared with the results of the corresponding QGSM calculations. It can be seen that the

Table 1: Experimental data on the inelastic density dn/dy for ϕ -meson production by the ALICE Collaboration at $\sqrt{s} = 2.76$ [37] and 7 TeV [38], compared with the results of the corresponding QGSM calculations.

Reactions	Energy \sqrt{s} , TeV	Experimental data on dn/dy ($ y \leq 0.5$)	QGSM
p + p	2.76	$0.0260 \pm 0.0004 \pm 0.003$ [37]	0.032
p + p	7.00	$0.032 \pm 0.0004 \pm 0.004$ [38]	0.05

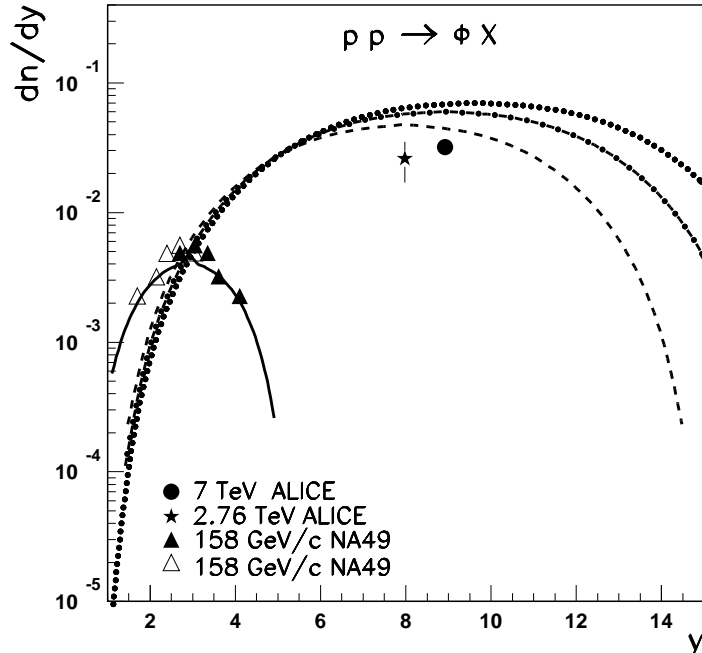


Figure 6: Experimental data [34, 35] on the y -spectra dn/dy of ϕ -mesons produced in pp collisions at 158 GeV/c, and the results of the corresponding calculation based on the QGSM (solid line). The dashed and dashed-dotted lines represent the results of the QGSM calculations at 2.76 and 7 Tev, and they are compared with corresponding experimental points in the central rapidity region, $|y| \leq 0.5$ [37, 38]. The dotted line is the QGSM prediction for 14 TeV.

QGSM results are rather higher than the experimental points. This is quite unexpected, since the QGSM calculations show in general a quite good agreement with the experimental data for proton-nucleus and nucleus-nucleus collisions both at RHIC and LHC energies (see next sections). May be, this is connected with the extrapolation to $p_T = 0$ of the experimental data actually measured at transverse momenta $p_T \geq 0.4$ GeV/c. The experimental data are shown in Table 1 as they are presented, after extrapolation, in the original experimental papers.

The energy dependence of the production cross section ratios of ϕ/π^- (upper panel) [41, 42] and ϕ/K^- (lower panel) [38, 41] in pp -collisions are presented in Fig. 8, where the corresponding QGSM description is shown by solid curves. The energy dependences of our curves for ϕ/π^- and ϕ/K^- are similar, since the ratio of K/π production depends rather weakly on the initial beam momentum.

One can see some disagreements of the QGSM curves with the data at high LHC energies. The ratios for ϕ/π^- and ϕ/K^- predicted by the QGSM increase from $\sqrt{s} = 0.9$ to 7 TeV, whereas for the experimental values the ratios are practically the same and do not grow with energy in the LHC energy range.

These discrepancies can also be connected with the influence of the kinematical boundaries at relatively low p_T , and they should be, at least in part, smaller when we

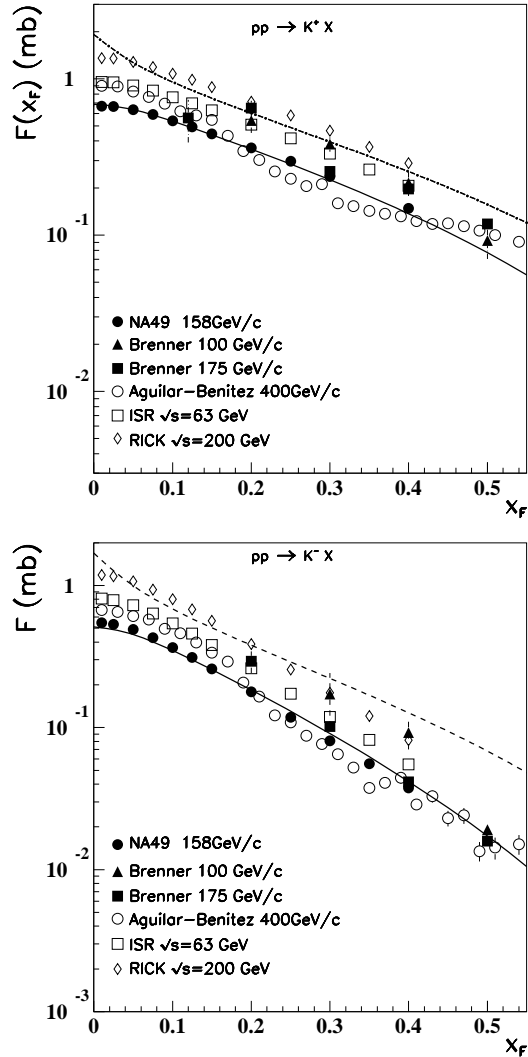


Figure 7: Experimental data on the invariant cross section of K^+ (upper panel) and K^- (lower panel) mesons produced in pp collisions at different energies [34, 35, 40] compared to the results of the corresponding calculations based on the QGSM. Solid lines correspond to the QGSM result at 158 GeV/c ($\sqrt{s} = 17.3$ GeV), while dashed lines correspond to the QGSM calculation at RHIC energy ($\sqrt{s} = 200$ GeV).

consider the ratios ϕ/π^- or ϕ/K^- with the same kinematical restrictions.

4 The ϕ -meson production in hadron collisions with nuclear targets up to RHIC energies

We analyze experimental data by the HERA-B Collaboration on ϕ -meson production in collisions of protons with C , Ti , and W nuclei. These data were integrated over the whole range of the transverse momentum p_T at $\sqrt{s} = 41.6$ GeV [43].

The A dependence of the cross section $d\sigma_{pA}/dy(y \simeq 0)$ is shown in Fig. 9 along

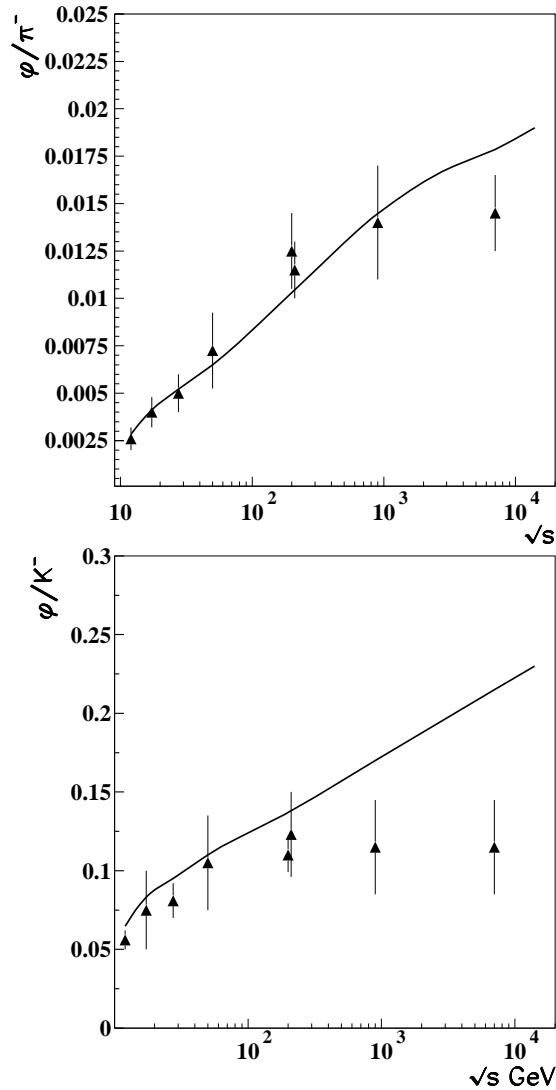


Figure 8: Experimental data [38, 41, 42] on the the \sqrt{s} dependence of ϕ/π^- (upper panel) and ϕ/K^- (lower panel) cross section ratios in pp collisions, compared to the results of the corresponding calculations based on QGSM.

with the results of corresponding calculations based on QGSM. These results are also presented in Table 2.

In Fig. 10, experimental data on the rapidity dependence of the inclusive cross section for ϕ -meson production, $d\sigma/dy$, in pA collisions for different C , Ti , and W targets, and for rather small rapidity ranges, are given along with the results of corresponding calculations based on the QGSM. The theoretical results compare reasonably with these experimental data everywhere, with the exception of some differences in the positive region of $y \geq 0$ that slightly increase with the atomic number A of the target, and that become more apparent for the W nucleus.

Table 2: The experimental data of the HERA-B Collaboration [43] on ϕ -meson production in pA collisions at $\sqrt{s} = 41.6$ GeV and the results of corresponding calculations based on the QGSM.

Reaction	Experimental data $d\sigma_{pA}/dy$ ($ y \leq 0.5$), mb	QGSM
p + C	1.74 ± 0.15	1.5
p + Ti	6.85 ± 0.7	7.1
p + W	23.5 ± 2.1	19.1

Table 3: Experimental values of dn/dy , $|y| \leq 0.5$, for ϕ -meson production in central nucleus-nucleus collisions at different energies, and results of corresponding calculations based on the QGSM.

Reaction	Centrality %	Energy \sqrt{s}, GeV	Experimental data on dn/dy ($ y \leq 0.5$)	QGSM
Pb + Pb	0–5%	17.3	2.35 ± 0.15 , [34, 35]	2.764
Au + Au	0–20%	62.4	$3.52 \pm 0.08 \pm 0.45$, [45]	3.36
Au + Au	0–11%	130.	$5.73 \pm 0.37, \pm 0.57$, [46, 47]	6.15
Au + Au	0–5%	200.	$7.95 \pm 0.11 \pm 0.73$, [45]	8.12
Au + Au	0–5%	200.	7.70 ± 0.30 , [41]	8.12

In the case of the production of particles such as pions and kaons, which make a dominant contribution to the mean multiplicity, a new shadowing effect, explained by A. Capella, A. Kaidalov, and J. Tran Thanh Van in ref. [44], appears starting from an energy of $\sqrt{s} = 40$ to 60 GeV.

In the case of ϕ -meson production this new screening effect is not noticeable, even in the region of the RHIC energies, but it appears at the LHC energies, which will be discussed in detail in the next section.

Let us now consider the experimental data on ϕ -meson production in heavy ion collisions at energies from $\sqrt{s} = 17.3$ to 200 GeV.

In Table 3, the experimental values of the midrapidity inclusive densities, dn/dy ($|y| \leq 0.5$), for ϕ -meson production in central nucleus-nucleus collisions, obtained by the NA49 Collaboration ($\sqrt{s} = 17.3$ GeV [34, 35]), and those obtained at RHIC (STAR and PHENIX Collaborations, $\sqrt{s} = 62.4$ GeV [45], 130 GeV [46, 47], and 200 GeV [41, 45]), are compared with the results of corresponding calculations. based on the QGSM.

Fig. 11 shows experimental data on the energy dependence of the inclusive den-

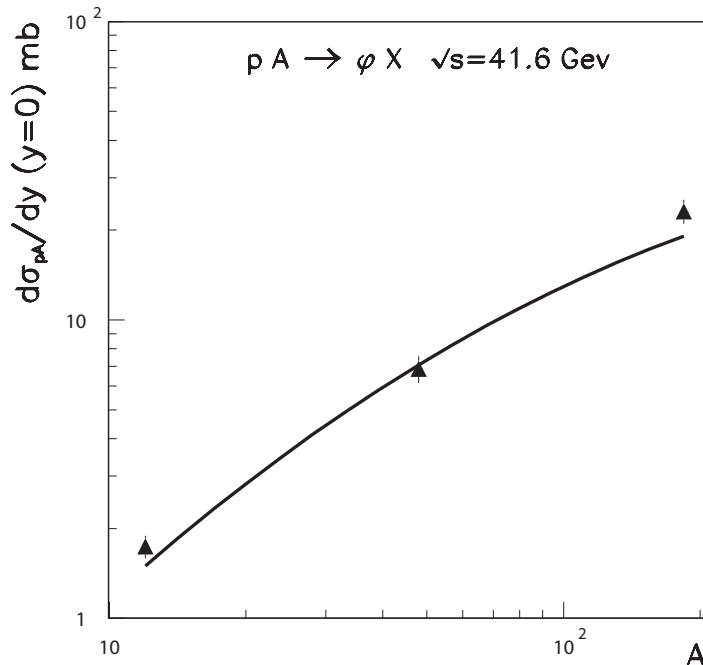


Figure 9: Experimental data on the A -dependence of the cross section for ϕ -meson production, $d\sigma_{pA}/dy$ ($y \simeq 0$), at the energy $\sqrt{s} = 41.6$ GeV [43] (triangles) and results of corresponding calculation based on the QGSM (curve).

sity in the midrapidity region, dn/dy ($y = 0$), in $PbPb$ (NA49 Collaboration, $\sqrt{s} = 17.3$ GeV [34, 35], closed box) and $AuAu$ collisions (STAR and PHENIX Collaborations, $\sqrt{s} = 62.4$ GeV [45], 130 [46, 47], and 200 GeV [41, 45], closed circles). The theoretical curve has been calculated for $AuAu$ collisions by using the QGSM formalism.

A rather strong energy dependence of the inclusive density being considered stems from the fact that the ϕ -meson mass is quite sizable, and thus the minimal value of x_{\pm} in Eq. (5) decreases substantially as the initial energy grows. This leads to the corresponding broadening of the integration domain in Eq. (6) and, accordingly, to the growth of the inclusive density in the midrapidity region.

Experimental data on the rapidity spectrum, dn/dy , of ϕ -mesons produced in $PbPb$ collisions at 158 GeV/c [34, 35] are shown in Fig. 12, along with the results of corresponding calculations based on the QGSM.

The agreement between the results of the theoretical calculations and experimental data is quite resonable at $y = 0$, but, as the rapidity y grows, the theoretical curve goes down more quickly than the experimental data. The reason for this possibly lies on the fact that at this energy it would be necessary to take into account the contribution of the quasi-two-particle channel, which should be considered separately.

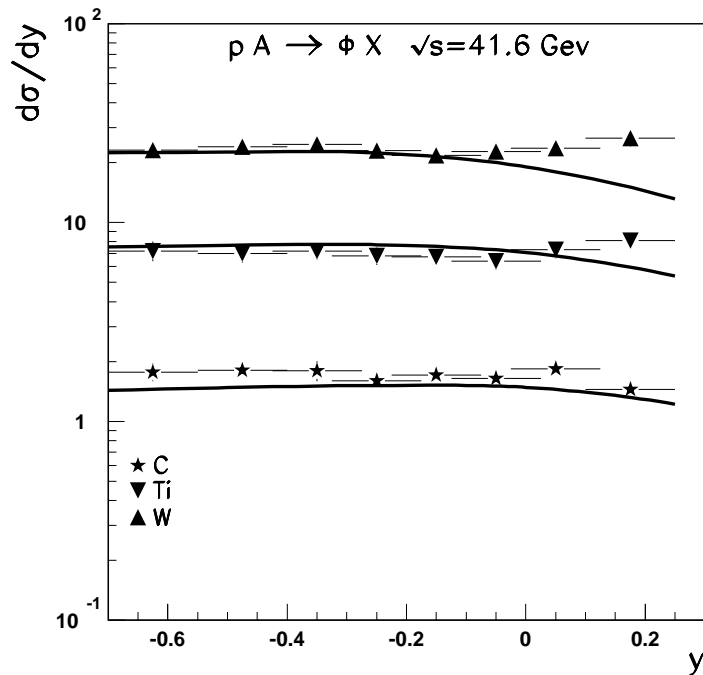


Figure 10: Experimental data on the y dependence of the cross section for ϕ -meson production, $d\sigma/dy$, in pA collisions on different nuclei ($A = C, Ti, W$), at the energy $\sqrt{s} = 41.6$ GeV [43] (points) and results of corresponding calculations based on QGSM (curves).

5 The ϕ -meson production on nuclear targets at LHC energies

In the previous section, it was shown that, in the case of ϕ -meson production, the inelastic-shadowing effects are very weak at RHIC energies, being virtually invisible against the experimental errors.

In this section we analyze the significance of the shadowing contribution for ϕ -meson production in the LHC energy range.

In ref. [44], it was explained that starting from RHIC energies, the inclusive density for the production of secondary particles exhibits significant saturation effects, both in pPb and in $PbPb$ collisions, what has been since experimentally confirmed [18, 48, 49].

Saturation effects can be explained by inelastic-shadowing corrections connected to the multipomeron interactions [44], which are negligible at low energies due to the suppression of the longitudinal part of the nuclear form factor.

In the case of interaction with nuclei, the mean number of Pomerons is large, and even at the RHIC and LHC energies their interactions become significant. Since the growth of the initial energy weakens the suppression of the longitudinal part of the

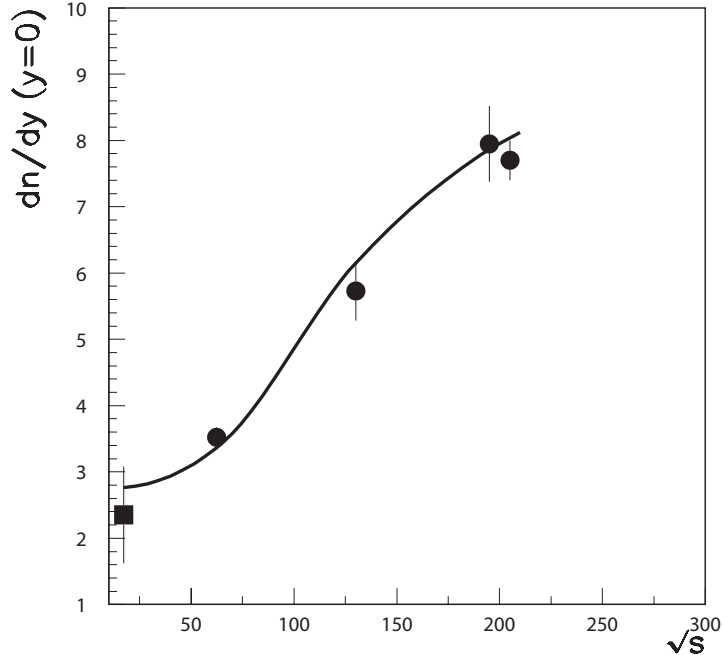


Figure 11: Experimental data on the energy dependence of inclusive density for ϕ -meson production in the midrapidity region, dn/dy , $|y| \sim 0$, in $PbPb$ (closed box) [34, 35] and $AuAu$ (closed circles) [41, 45, 46] collisions. The theoretical curve represents the results of corresponding calculations for $AuAu$ collisions based on the QGSM

nuclear factor, the inelastic-shadowing corrections become more and more significant as the initial energy increases.

The calculations of inclusive densities and multiplicities can be performed in the percolation approach (with accounting for the inelastic shadowing) in both pp [50, 51] and heavy ion collisions [51, 52]. The results of these calculations are in good agreement with the experimental data over a broad energy region.

The percolation approach assumes that two or several Pomerons overlap one another in the transverse space and merge together in a single Pomeron. As a result, and given a certain value of the transverse radius of the interaction region, when the density of Pomerons in that interaction region becomes large enough, internal partons (quarks and gluons) from different nucleons can merge, leading to the saturation of the inclusive density of final-state particles. As the energy grows, this effect persists up to the overlap of all Pomerons [53, 54, 55].

Technically, a more direct way to take into account the percolation effects in the QGSM [18] is to consider the maximal number of cut Pomerons in the midrapidity region, n_{max} , that were emitted by one nucleon. If the number of emitted Pomerons is less than n_{max} , then different final states of produced particles arise upon cutting them. The contributions of all the diagrams with $n \leq n_{max}$ are then taken into account in just the same way as at low energies. According to the unitarity constraint, a larger number of Pomerons $n > n_{max}$ can be emitted. Because of final-state interaction

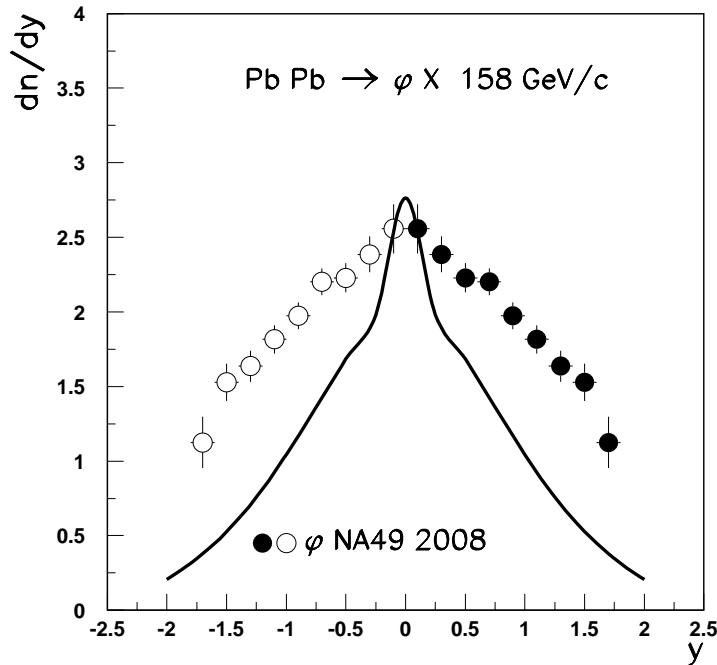


Figure 12: Experimental data on the rapidity dependence of the density for ϕ -meson production, dn/dy , in $PbPb$ collisions at the momentum of 158 GeV/c [34, 35] (points) along with the results of corresponding calculation based on the QGSM.

(merger), however, the same final state as in the case of cutting n_{max} Pomerons arises upon cutting these Pomerons at the quark-gluon stage.

With this prescription, the QGSM calculations become straightforward, and their results are similar to those of calculations in the percolation model. According to this scenario, the QGSM provides a reasonable agreement with the experimental data on the inclusive spectra of light secondary particles at a value $n_{max} = 13$ in the case of RHIC energies (see ref. [18]), and at $n_{max} = 21$ in the case of LHC energies [56]. These values of n_{max} reflect the fact that the merger of Pomerons is quite efficient in the case of π^\pm , K^\pm , p , and \bar{p} production. In the absence of inelastic shadowing, the maximal number of Pomerons is substantially larger, which leads to higher values of inclusive densities [17, 18].

The number of strings that determines particle production grows with increasing initial energy even if the percolation effects are included. This was explained in ref. [57]. The point is that the number of Pomerons that could make a significant contribution to the spectra in the absence of inelastic shadowing grows fast with increasing initial energy, and an increase in the value of the parameter n_{max} does not prevent the growth of the relative contribution of inelastic shadowing.

Below we compare the experimental data on ϕ -meson production in collisions on nuclear targets at LHC energies, with the results of the corresponding QGSM calcula-

tions.

In Fig. 13 we present the result of the QGSM calculations for the rapidity dependence of the density dn/dy of ϕ -meson production in $PbPb$ collisions, for centrality 5% with (solid curve) and without (dashed curve) including the inelastic-shadowing effect. One can see that the inelastic-shadowing contribution is sizable in the midrapidity region, but it decreases sharply as the rapidity y grows. Also in Fig. 13, the QGSM prediction [2] is compared with the experimental point on dn/dy at $y = 0$ for ϕ -meson production at $\sqrt{s} = 2.76$ TeV recently published by the ALICE Collaboration [58].

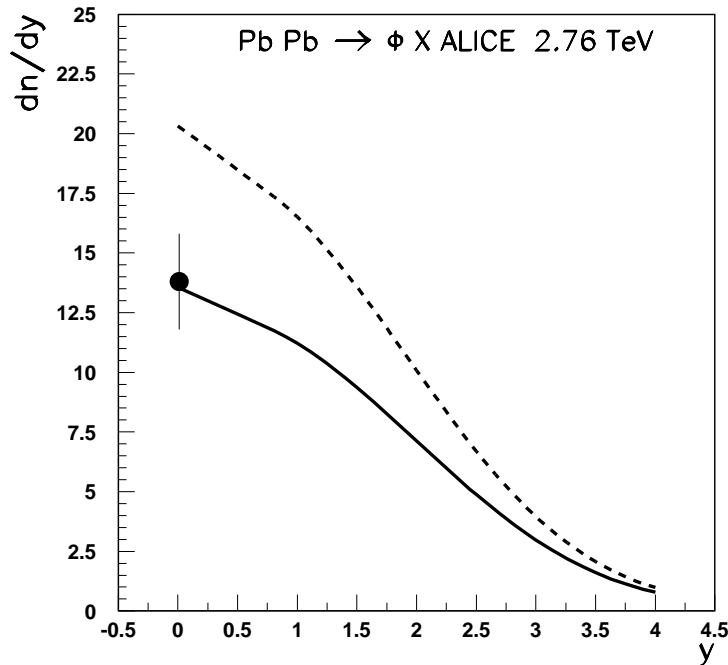


Figure 13: Comparison of the QGSM prediction for the rapidity dependence of the density of ϕ -meson production, dn/dy , in central $PbPb$ collisions at $\sqrt{s} = 2.76$ TeV (solid curve) with one experimental point by ALICE Collaboration [58]. The dashed curve represents the result of the QGSM calculation without including the inelastic-shadowing effect.

In Table 4 we present the results of the QGSM calculations for LHC energies, obtained without using any additional parameter with respect to the calculations at lower energies, so these results can be considered as theoretical predictions. The comparison with the corresponding available experimental data is also shown. Unfortunately, only one experimental point by the ALICE Collaboration [58] is currently available on the ϕ -meson production density dn/dy ($|y| \leq 0.5$) in $PbPb$ collisions at $\sqrt{s} = 2.76$ TeV and centrality 5%, and the same occurs for ϕ -meson production in pPb collisions at $\sqrt{s} = 5.02$ TeV for non-single diffraction (NSD) events [59].

When comparing the experimental point by the ALICE Collaboration [58] on the

Table 4: Experimental point by the ALICE Collaboration [58] on dn/dy , $|y| \leq 0.5$, for ϕ -meson production in $PbPb$ collisions at $\sqrt{s} = 2.76$ TeV, compared to the result of corresponding QGSM calculation. We also compare the QGSM result with the experimental point on pPb collisions at $\sqrt{s} = 5.02$ TeV, for non-single diffraction (NSD) events [59].

Reactions	Centrality	Energy \sqrt{s}, TeV	Experimental data $dn/dy (y \leq 0.5)$	QGSM
Pb + Pb	0–5%	2.76	$13.8 \pm 0.5 \pm 1.7 \pm 0.1$ [58]	13.57
p + Pb	NSD	5.02	$0.1344 \pm 0.005 \pm 0.0069 \pm 0.0081$ [59]	0.14

ϕ -meson production density dn/dy ($|y| \leq 0.5$) in $PbPb$ collisions at $\sqrt{s} = 2.76$ TeV and centrality 5%, with the result of corresponding QGSM calculation, the value of dn/dy ($|y| \leq 0.5$) = 13.57 is obtained, which agrees with the experimental data, at $n_{max} = 37$. The calculation at an asymptotically large value of n_{max} (that is, in the absence of inelastic shadowing), yields a value of dn/dy ($|y| \leq 0.5$) $\simeq 20.5$. The inelastic-shadowing effect reduces the value of dn/dy ($|y| \leq 0.5$) by about 1.5. At this energy, the π^\pm , K^\pm , p , and \bar{p} spectra decrease by a factor of about two because of a larger contribution of inelastic shadowing.

On the other hand, the QGSM calculation for the density dn/dy of ϕ mesons produced in pPb collisions at $\sqrt{s} = 5.02$ TeV, to compare with the corresponding experimental point by the ALICE Collaboration [59] at the same energy, for non-single diffraction (NSD) events, were made with $n_{max} = 32$. The different values of n_{max} are connected with different initial beams (the number of cutted Pomerons in $PbPb$ and pPb collisions) and with different initial energies.

Since once the value of n_{max} is fixed, the secondary ϕ -meson production in proton-nucleus and nucleus-nucleus collisions can be calculated without any additional parameter with respect to the corresponding calculations for pp collisions.

As we can see in Table 4, QGSM gives a rather good description of these ALICE Collaboration points, but, of course, new experimental data on ϕ -meson production at LHC energies, both for pPb and $PbPb$ collisions, will be crucial in order to draw final conclusions.

6 Conclusions

The QGSM provides a reasonable description of Feynman x_F and rapidity y spectra of ϕ -meson production for the interaction of different hadron beams with a nucleon target in a wide energy region, by using for the only unknown parameter in the QGSM analysis, the normalization parameter a_ϕ . The value $a_\phi = 0.11$ is determined by comparison with experimental data in the energy range up to RHIC, where the screenig contri-

bution is negligible for ϕ -meson production, and then used for ϕ -meson production processes at higher energies.

At LHC energies, a new parameter n_{max} , connected with the number of cut pomerons, appears in the calculation of the inelastic nuclear shadowing contribution to ϕ -meson production.

The QGSM prediction for the density dn/dy at LHC energies in pp collisions are compared with recent experimental data at $\sqrt{s} = 2.76$ and 7 TeV in the midrapidity region. The theoretical results based on the QGSM calculations for the ϕ/π^- and ϕ/K^- cross section ratios present a reasonable agreement with the corresponding experimental data in a wide interval of the beam energy, going up to the LHC range. Since the theoretical ratios ϕ/π^- and ϕ/K^- grow with energy from $\sqrt{s} = 0.9$ to 7 TeV, while the experimental points do not show this growth, and, since, in particular, the prediction based on the QGSM for the ratio ϕ/π^- at $\sqrt{s} = 0.9$ TeV is in agreement with the experiment, some discrepancy of the QGSM calculations with the experimental data appearing at the LHC energy of $\sqrt{s} = 7$ TeV.

Concerning the interactions of protons and nuclei with nuclear targets, the QGSM provides a reasonable description of ϕ -meson production up to the RHIC energies without recourse to any additional parameter, and without the inclusion of inelastic-shadowing effects.

The effect of inelastic nuclear shadowing is markedly weaker in the case of ϕ -meson production than in the case of the production of other particles, such as π^\pm , K^\pm , p , and \bar{p} , and becomes observable at higher energies of $\sqrt{s} \geq 0.9$ TeV. This behaviour can be explained by the fact that the mass of the strange quark is not very small.

Acknowledgements This work has been supported by Russian RSCF grant No. 14-22-00281, by Ministerio de Ciencia e Innovación of Spain under project FPA2014-58293-C2-1-P, and Maria de Maeztu Unit of Excellence MDM-2016-0692, and by Xunta de Galicia, Spain, under 2015-AEFIS (2015-PG034), AGRUP2015/11.

Appendix A: Pomeron pole and multipomeron-exchange cross sections

The detailed description of the process of construction of the multipomeron-exchange amplitude for hadron-hadron scattering at high energies in the classical reggeon diagram technique is given in references [1, 3, 4, 14, 60].

In the case of a supercritical Pomeron with

$$\alpha_P(t) = 1 + \Delta + \alpha'_P t, \quad \Delta > 0, \quad (\text{A.1})$$

one obtains the correct asymptotic behaviour, $\sigma_{tot} \sim \ln^2 s$. The one-Pomeron contri-

bution to σ_{hN}^{tot} equals:

$$\sigma_P = 8\pi\gamma e^{\Delta\xi}, \quad \xi = \ln s/s_0, \quad (\text{A.2})$$

where γ is the Pomeron coupling, and σ_P rises with energy as s^Δ . To obey the s -channel unitarity, and the Froissart bound in particular, this contribution should be screened by the multipomeron discontinuities. A simple quasi-eikonal treatment [21] yields:

$$\sigma_{hN}^{tot} = \sigma_P f(z/2), \quad \sigma_{hN}^{el} = \frac{\sigma_P}{C} [f(z/2) - f(z)], \quad (\text{A.3})$$

where

$$f(z) = \sum_{k=1}^{\infty} \frac{1}{k \cdot k!} (-z)^{k-1} = \frac{1}{z} \int_0^z \frac{dx}{x} (1 - e^{-x}), \quad (\text{A.4})$$

$$z = \frac{2C\gamma}{\lambda} e^{\Delta\xi}, \quad \lambda = R^2 + \alpha'_P \xi. \quad (\text{A.5})$$

Here, R^2 is the radius of the Pomeron, and C is the quasi-eikonal enhancement coefficient (see [61]). At asymptotically high energies ($z \gg 1$), we obtain:

$$\sigma_{hN}^{tot} = \frac{8\pi\alpha'_P\Delta}{C} \xi^2, \quad \sigma_{hN}^{el} = \frac{4\pi\alpha'_P\Delta}{C^2} \xi^2, \quad (\text{A.6})$$

according to the Froissart limit [62].

The values of Pomeron parameters were fixed in [1, 6] on the base of a Regge fit [60] of high-energy hadron-nucleon scattering, by including into the analysis the by then new data from colliders:

$$\Delta = 0.139, \quad \alpha'_P = 0.21 \text{ GeV}^{-2}, \quad (\text{A.7})$$

$$\gamma_{pp} = 1.77 \text{ GeV}^{-2}, \quad R_{pp}^2 = 3.18 \text{ GeV}^{-2}, \quad C_{pp} = 1.5,$$

$$\gamma_{\pi p} = 1.07 \text{ GeV}^{-2}, \quad R_{\pi p}^2 = 2.48 \text{ GeV}^{-2}, \quad C_{\pi p} = 1.65.$$

The error bars of the parameters are not presented, since they are strongly correlated. With these values for the set of parameters in pp collisions, one obtains a value of $\sigma_{pp}^{tot} \simeq 94$ mb at the LHC energy of $\sqrt{s} = 7$ TeV, that is only slightly smaller than the experimental value $\sigma_{pp}^{tot} = 98.3 \pm 2.8$ mb [63].

Appendix B: Quark and diquark distributions in hadrons in QGSM

The QGSM considers hadrons as consisting of constituent quarks, so we cannot use hadron structure functions obtained from hard processes. Usually, it is assumed in DTU that a proton consists of a valence quark q and a diquark qq . The diquark qq contains not only two valence quarks, but also some part of gluon field, in what is

called string junction (SJ) [64, 65]. In this case, the diquark average momentum is larger than twice the momentum of a valence quark. In the QGSM a proton can also contain several sea quark-antiquark pairs.

In QGSM the form of the functions $u(x, n)$ is determined by the corresponding Regge asymptotic behaviours in the regions $x \rightarrow 0$ and $x \rightarrow 1$ [66, 67]. As an example, let us consider the diagram with annihilation of one quark from the fast nucleon on a meson target, that is shown in Fig. 14a.

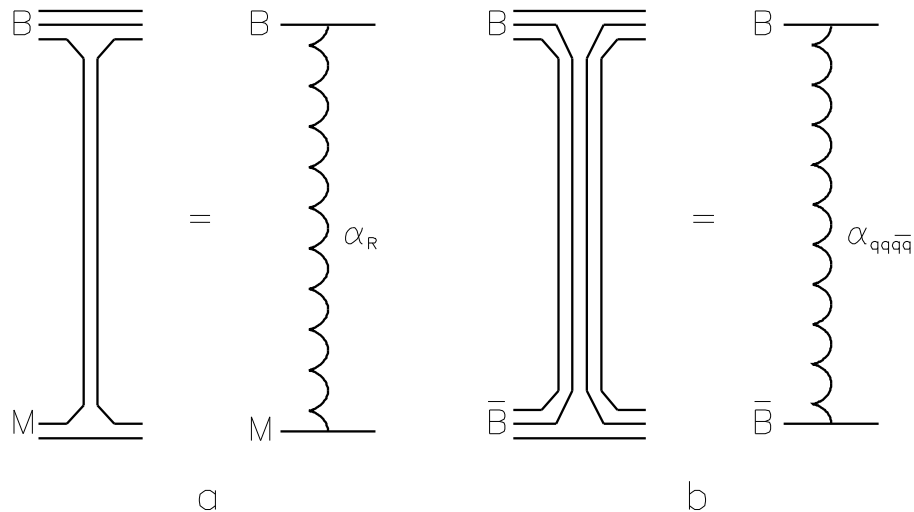


Figure 14: Planar diagrams which determine the low- x asymptotic behaviour (a) of the valence quark distribution in a nucleon, and (b) of the diquark distribution in a nucleon.

The contribution of this process to the total inelastic hN cross section is proportional to $e^{[\alpha_R(0)-1]\Delta y}$, where $\alpha_R(0) \simeq 0.5$ is the intercept parameter of the corresponding non-vacuum Regge trajectory, and Δy is the difference between the rapidities of the colliding particles. On the other hand, and starting from the parton model, we can consider this process from a different point of view [67]; *i.e.*, a slow valence quark exists in the incident fast nucleon that is Δy rapidity distant away from the valence diquark, the probability of such a configuration depending on Δy . This slow valence quark annihilates with a target antiquark with a rather large probability, what corresponds to the cut of the diagram in Fig. 14a. Then, the probability to find a slow valence quark in the fast nucleon at a distance Δy , *i.e.* with $x \simeq e^{-\Delta y} \rightarrow 0$, is equal to

$$xu_q(x) \sim x^{1-\alpha_R(0)}, \quad x \rightarrow 0. \quad (\text{B.1})$$

The probability of finding a valence quark with $x \rightarrow 1$ in the nucleon is determined by the probability of finding a slow diquark. This can be detected in the process of $N\bar{N}$ annihilation that is shown in Fig. 14b. The intercept of the corresponding

Regge trajectory $\alpha_{qq\bar{q}\bar{q}}$ can be calculated as [22, 67] $\alpha_{qq\bar{q}\bar{q}}(0) = -\alpha_R(0) + 2\alpha_B(0)$, where $\alpha_B(0) \simeq -0.5$ is a parameter of the nucleon Regge trajectory. Then,

$$xu_q(x) \sim (1-x)^{1+\alpha_R(0)-2\alpha_B(0)}, \quad x \rightarrow 1. \quad (\text{B.2})$$

The quark distribution in the intermediate x region can be estimated with the help of a simple interpolation,

$$u(x) = Cx^\alpha(1-x)^\beta, \quad (\text{B.3})$$

with both limits at $x \rightarrow 0$ and $x \rightarrow 1$ given by eqs. B.1 and B.2. The normalization factor C is determined by the condition

$$\int u_i(x, n) dx = 1, \quad (\text{B.4})$$

leading to

$$C = \frac{\Gamma(\alpha + \beta + 2)}{\Gamma(\alpha + 1)\Gamma(\beta + 1)}. \quad (\text{B.5})$$

The numerical calculations account for the fact that the distribution of valence d -quark in the proton is softer than the distribution of valence u -quarks. This can be done by including into $u_d(x, n)$ an additional factor $(1-x)$ with respect to $u_u(x, n)$. The diquark distributions can be derived from the quark distributions by substituting $x \rightarrow (1-x)$.

The diquark and quark distribution functions depend on the number n of cut Pomerons in the diagrams being considered.

As a consequence of momentum conservation, for each value of n one has

$$\sum_i \langle x_i \rangle = \sum_i \int u_i(x, n) x dx = 1. \quad (\text{B.6})$$

In the case of $n > 1$, *i.e.*, for multipomeron exchange the distributions of valence quarks and diquarks are softened with respect to the case of $n = 1$, due to the appearance of a sea quark contribution. For arbitrary n , one has [14]:

$$u_{uu}(x, n) = C_{uu} x^{\alpha_R - 2\alpha_B + 1} (1-x)^{-\alpha_R + \frac{4}{3}(n-1)}, \quad (\text{B.7})$$

$$u_{ud}(x, n) = C_{ud} x^{\alpha_R - 2\alpha_B} (1-x)^{-\alpha_R + n - 1}, \quad (\text{B.8})$$

$$u_u(x, n) = C_u x^{-\alpha_R} (1-x)^{\alpha_R - 2\alpha_B + n - 1}, \quad (\text{B.9})$$

$$u_d(x, n) = C_d x^{-\alpha_R} (1-x)^{\alpha_R - 2\alpha_B + 1 + \frac{4}{3}(n-1)}, \quad (\text{B.10})$$

$$u_s(x, n) = C_d x^{-\alpha_R} (1-x)^{\alpha_R - 2\alpha_B + n - 1}. \quad (\text{B.11})$$

The quark distributions in pion can be obtained in a similar way, *e.g.*, for the case of π^- mesons, we use the distributions [14]:

$$u_d(x, n) = u_{\bar{u}}(x, n) = C_d x^{-\alpha_R} (1-x)^{-\alpha_R + n - 1}, \quad (\text{B.12})$$

$$u_u(x, n) = u_{\bar{d}}(x, n) = C_u x^{-\alpha_R} (1-x)^{-\alpha_R + n - 1} [1 - \delta \sqrt{1-x}], \quad n > 1, \quad (\text{B.13})$$

$$u_{\bar{s}}(x, n) = C_{\bar{s}} x^{-\alpha_R} (1-x)^{n-1}, \quad n > 1. \quad (\text{B.14})$$

Appendix C: Quark and diquark fragmentation functions in vector ϕ -mesons in QGSM

First, it has to be noted that the fragmentation functions $G_i^h(z)$ used in QGSM are related to the standard fragmentation functions $D(z)$ by the equation $G(z) = zD(z)$ [4, 22].

For the ϕ -meson production we use the following quark fragmentation functions [10], that were obtained by using the Reggeon counting rules and the simplest extrapolation [22]:

$$G_u^\phi = G_d^\phi = G_{\bar{u}}^\phi = G_{\bar{d}}^\phi = a_\phi \cdot (1-z)^{\lambda-\alpha_R-2\alpha_\phi+2}, \quad (\text{C.1})$$

$$G_s^\phi = G_{\bar{s}}^\phi = a_\phi \cdot (1-z)^{\lambda-\alpha_\phi}. \quad (\text{C.2})$$

The diquark fragmentation functions into ϕ -mesons have the form:

$$G_{uu}^\phi = G_{ud}^\phi = a_\phi \cdot (1-z)^{\lambda+\alpha_R-2(\alpha_R+\alpha_\phi)}, \quad (\text{C.3})$$

where parameters $\alpha_R = 0.5$ and $\alpha_\phi = 0$. are the intercepts of the ρ and ϕ Regge trajectories, respectively.

The parameter λ is $\lambda = 2\alpha'_R < p_T^2 >$, where α'_R is the slope of the vector-meson trajectory, and $< p_T^2 >$ is the average square transverse momenta of the produced mesons.

The only unknown value in the model is that of parameter a_ϕ , which corresponds the normalisation of the ϕ density in the central region of rapidity y . This value is universal in the sense that it does not depend, neither of the energy, nor of the beam and target types of the collision processes. The value of a_ϕ has been determined by comparing the results of the model calculations with the available experimental data on ϕ production from pion and proton beams (see section 3). Thus, in the calculations we present here the value of $a_\phi = 0.11$, which gives a good description of most of those experimental data, has been used.

References

- [1] G.H. Arakelyan, C. Merino, and Yu.M. Shabelski, Phys. Rev. **D90**, 114019 (2014), doi:10.1103/PhysRevD.95.074013, and arXiv:1604.01918[hep-ph].
- [2] G.H. Arakelyan, C. Merino, and Yu.M. Shabelski, Phys. At. Nucl. **80**, 1197 (2017) and Yad. Fiz. **80**, 719 (2017), arXiv:1610.06039[nucl-th].
- [3] A.B. Kaidalov and K.A. Ter-Martirosyan, Sov. J. Nucl. Phys. **39**, 979 (1984) and Yad. Fiz. **39**, 1545 (1984); Sov. J. Nucl. Phys. **40**, 135 (1984) and Yad. Fiz. **40**, 211 (1984).

- [4] A.B. Kaidalov, Phys. At. Nucl. **66**, 1994 (2003), doi:10.1134/1.1625743.
- [5] A.B. Kaidalov and O.I. Piskounova, Sov. J. Nucl. Phys. **41**, 816 (1985) and Yad. Fiz. **41**, 1278 (1985).
- [6] Yu.M. Shabelski, Sov. J. Nucl. Phys. **44**, 117 (1986) and Yad. Fiz. **44**, 186 (1986).
- [7] C. Merino, C. Pajares and Yu.M. Shabelski, Eur. Phys. J. **C73**, 2266 (2013), doi:10.1140/epjc/s10052-012-2266-9, and arXiv:1207.6900[hep-ph].
- [8] G.H. Arakelyan, C. Merino, C. Pajares, and Yu.M. Shabelski, Eur. Phys. J. **C54**, 577 (2008), doi:10.1140/epjc/s10052-008-0554-1, and arXiv:0709.3174[hep-ph].
- [9] G.H. Arakelyan, C. Merino, C. Pajares, and Yu.M. Shabelski, Eur. Phys. J. **A31**, 519 (2007), doi:10.1140/epja/i2006-10282-6, and arXiv:0610.264[hep-ph].
- [10] G.H. Arakelyan, Sh.S. Eremian, Phys. Atom. Nucl. **58**, 1241 (1995) and Yad. Fiz. **58**, 132 (1995).
- [11] G.H. Arakelyan, C. Pajares, and Yu.M. Shabelski, Z. Phys. **C73**, 697 (1997), doi:10.1007/s002880050361, and hep-ph/9602348.
- [12] G.H. Arakelyan, A. Capella, A.B. Kaidalov, and Yu.M. Shabelski, Eur. Phys. J. **C26**, 81 (2002), doi:10.1007/s10052-002-0977-z, and arXiv:0103.337[hep-ph].
- [13] G.H. Arakelyan, A.B. Kaidalov, C. Merino, and Yu.M. Shabelski, Phys. Atom. Nucl. **74**, 426 (2011), doi:10.1134/S1063778811030057, and arXiv:1004.4074[hep-ph].
- [14] A.B. Kaidalov, K.A. Ter-Martirosyan, and Yu.M. Shabelski, Sov. J. Nucl. Phys. **43**, 822 (1986) and Yad. Fiz. **43**, 1282 (1986).
- [15] Yu.M. Shabelski, Z. Phys. **C38**, 569 (1988), doi:10.1007/BF01624362.
- [16] Yu.M. Shabelski, Sov. J. Nucl. Phys. **50**, 149 (1989) and Yad. Fiz. **50**, 239 (1989).
- [17] G.H. Arakelyan, C. Merino, C. Pajares, and Yu.M. Shabelski, Phys. Atom. Nucl. **76**, 316 (2013) and Yad. Fiz. **76**, 348 (2013), doi:10.1134/S1063778813020026, and arXiv:1207.6899[hep-ph].
- [18] C. Merino, C. Pajares, and Yu.M. Shabelski, Eur. Phys. J. **C59**, 691 (2009), doi:10.1140/epjc/s10052-008-0810-4, and arXiv:0802.2195[hep-ph].
- [19] G.H. Arakelyan, C. Merino, and Yu.M. Shabelski, Eur. Phys. J. **A52**, 9 (2016), doi:10.1140/epja/i2016-16009-2, and arXiv:1509.05218[hep-ph].
- [20] V.A. Abramovsky, V.N. Gribov, and O.V. Kancheli, Sov. J. Nucl. Phys. **18**, 308 (1974) and Yad. Fiz. **18**, 595 (1973).

- [21] K.A. Ter-Martirosyan, Phys. Lett. **B44**, 377 (1973), doi:10.1016/0370-2693(73)90411-5.
- [22] A.B. Kaidalov, Sov. J. Nucl. Phys. **45**, 902 (1987) and Yad. Fiz. **45**, 1452 (1987).
- [23] Yu.M. Shabelski, Sov. J. Nucl. Phys. **26**, 573 (1977) and Yad. Fiz. **26**, 1084 (1977); Nucl. Phys. **B132**, 491 (1978), doi:10.1016/0550-3213(78)90473-X.
- [24] L. Bertocchi and D. Treleani, J. Phys. **G3**, 147 (1977), doi:10.1088/0305-4616/3/2/007.
- [25] J.H. Weis, Acta Phys. Polonica **B7**, 851 (1976).
- [26] T. Jaroszewicz *et al.*, Z. Phys. **C1**, 181 (1979), doi:10.1007/BF01445409.
- [27] V.M. Braun and Yu.M. Shabelski, Int. J. Mod. Phys. **A3**, 2417 (1988), doi:10.1142/S0217751X8800103X.
- [28] G.D. Alkhozov *et al.*, Nucl. Phys. **A280**, 330 (1977), doi:10.1016/0375-9474(77)90609-1.
- [29] Yu.M. Shabelski, Z. Phys. **C57**, 409 (1993), doi:10.1007/BF01474336.
- [30] J. Dias de Deus and Yu.M. Shabelski, Phys. Atom. Nucl. **71**, 190 (2008) and Yad. Fiz. **71**, 191 (2008), doi:10.1007/s11450-008-1021-z,10.1134/S1063778808010213, and hep-ph/0612346.
- [31] C. Daum *et al.*, ACCMOR Collaboration, Nucl. Phys. **B186**, 205 (1981), doi:10.1016/0550-3213(81)90067-5.
- [32] R.J. Apsimon *et al.*, Omega-Photon Collaboration, Z. Phys. **C61**, 383 (1994), doi:10.1007/BF01413177; F-D. Gebert, Bonn-IR-92-10 (1992).
- [33] H. Dijkstra *et al.*, ACCMOR Collaboration, Z. Phys. **C31**, 375 (1986), doi:10.1007/BF01588035.
- [34] S.V. Afanasev *et al.*, NA49 Collaboration, Phys. Lett. **B491**, 59 (2000), doi:10.1016/S0370-2693(00)01023-6.
- [35] T. Anticic *et al.*, NA49 Collaboration, Eur. Phys. J. **C68**, 1 (2010), doi:10.1140/epjc/s10052-010-1328-0, and arXiv:1004.1889[hep-ex].
- [36] M. Atayan and H. Gulkanyan, hep-ex/0501024.
- [37] J. Adam *et al.*, ALICE Collaboration, Phys. Rev. **C95**, 064606 (2017), doi:10.1103/PhysRevC.95.064606, and arXiv:1702.00555[nucl-ex].
- [38] B. Abelev *et al.*, ALICE Collaboration, Eur. Phys. J. **C72**, 2183 (2012), doi:10.1140/epjc/s10052-012-2183-y, and arXiv:1208.5717[hep-ex].

- [39] C. Merino, C. Pajares, and Yu.M. Shabelski, Eur. Phys. J. **C71**, 1652 (2011), doi:10.1140/epjc/s10052-011-1652-z.
- [40] A.E. Brenner *et al.*, Phys. Rev. **D26**, 1497 (1982), doi:10.1103/PhysRevD.26.1497.
- [41] J. Adams *et al.*, STAR Collaboration, Phys. Lett. **B612**, 181 (2005), doi:10.1016/j.physletb.2004.12.082, and nucl-ex/:0406003.
- [42] B. Abelev *et al.*, ALICE Collaboration, Phys. Lett. **B710**, 557 (2012), doi:10.1016/j.physletb.2012.03.038, and arXiv:1112.2222[hep-ex].
- [43] I. Abt *et al.*, HERA-B Collaboration, Eur. Phys. J. **C50**, 315 (2007), doi:10.1140/epjc/s10052-007-0237-3, and hep-ex/0606049.
- [44] A. Capella, A. Kaidalov, and J. Tran Thanh Van, Acta Physica Hungarica-Heavy Ion Phys. **A9**, 169 (1999), and hep-ph/9903244.
- [45] B.I. Abelev *et al.*, STAR Collaboration, Phys. Rev. **C79**, 064903 (2009), doi:10.1103/PhysRevC.79.064903, and arXiv:0809.4737[nucl-ex].
- [46] K. Adcox *at al.*, PHENIX Collaboration, Phys. Rev. **C69**, 024904 (2004), doi:10.1103/PhysRevC.69.024904, and nucl-ex/0307010.
- [47] C. Adler *at al.*, STAR Collaboration, Phys. Rev. **C65**, 041901 (2002), doi:10.1103/PhysRevC.65.041901.
- [48] B.B. Back *et al.*, PHOBOS Collaboration, Phys. Rev. Lett. **85**, 3100 (2000), doi:10.1103/PhysRevLett.85.3100, and hep-ex/0007036.
- [49] K. Adcox *at al.*, PHENIX Collaboration, Phys. Rev. Lett. **86**, 3500 (2001), doi:10.1103/PhysRevLett.86.3500, and nucl-ex/0012008.
- [50] I. Bautista, C. Pajares, and J. Dias de Deus, Nucl. Phys. **A882**, 44 (2012), doi:10.1016/j.nuclphysa.2012.03.003, and arXiv:1110.4740[nucl-th].
- [51] I. Bautista, J. Dias de Deus, G. Milhano, and C. Pajares, Phys. Lett. **B715**, 230 (2012), doi:10.1016/j.physletb.2012.07.029, and arXiv:1204.1457[nucl-th].
- [52] I. Bautista, C. Pajares, G. Milhano, and J. Dias de Deus, Phys. Rev. **C86**, 034909 (2012), doi:10.1103/PhysRevC.86.034909, and arXiv:1206.6737[nucl-th].
- [53] J. Dias de Deus, E.G. Ferreira, C. Pajares, and R. Ugoccioni, Eur. Phys. J. **C40**, 229 (2005), doi:10.1140/epjc/s2005-02127-y, and hep-ph/0304068.
- [54] C. Pajares, Eur. Phys. J. **C43**, 9 (2005), doi:10.1140/epjc/s2005-02179-y, and hep-ph/0501125.
- [55] M.A. Braun, E.G. Ferreira, F. del Moral, and C. Pajares, Eur. Phys. J. **C25**, 249 (2002), doi:10.1007/s10052-002-0989-8, and hep-ph/0111378.

- [56] C. Merino, C. Pajares, and Yu.M. Shabelski, *Eur. Phys. J.* **C73**, 2266 (2013).
- [57] J. Dias de Deus and C. Pajares, *Phys. Lett.* **B695**, 211 (2012), doi:10.1016/j.physletb.2010.11.017, and arXiv:1011.1099[hep-ph].
- [58] B. Abelev *et al.*, ALICE Collaboration, *Phys. Rev.* **C91**, 024609 (2015), doi:10.1103/PhysRevC.91.024609, and arXiv:1404.0495[nucl-ex].
- [59] J. Adam *et al.*, ALICE Collaboration, *Eur. Phys. J.* **C76**, 245 (2016), doi:10.1140/epjc/s10052-016-4088-7, and arXiv:1601.07868.
- [60] A.M. Lapidus, V.I. Lisin, K.A. Ter-Martirosyan, and P.E. Volkovitsky, *Sov. J. Nucl. Phys.* **24**, 468 (1976) and *Yad. Fiz.* **24**, 1237 (1976).
- [61] K.A. Ter-Martirosyan, *Sov. J. Nucl. Phys.* **10**, 600 (1970) and *Yad. Fiz.* **10**, 1047 (1969).
- [62] M. Froissart, *Phys. Rev.* **123**, 1053 (1961), doi:10.1103/PhysRev.123.1053.
- [63] G. Antchev *et al.*, TOTEM Collaboration, *Europhys. Lett.* **95**, 41001 (2011), doi:10.1209/0295-5075/95/41001, and arXiv:1110.1385[hep-ex].
- [64] M. Imachi, S. Otsuki, and F. Toyoda, *Progr. Theor. Phys.* **54**, 280 (1975), doi:10.1143/PTP.54.280; **55**, 551 (1976), doi:10.1143/PTP.55.551.
- [65] G.C. Rossi and G. Veneziano, *Nucl. Phys.* **B123**, 507 (1977), doi:10.1016/0550-3213(77)90178-X.
- [66] A. Capella, U. Sukhatme and J. Tran Thanh Van, *Z. Phys.* **C3**, 329 (1980), doi:10.1007/BF01414185.
- [67] A.B. Kaidalov, *Z. Phys.* **C12**, 63 (1982), doi:10.1007/BF01475732.